Classification of plasmodium falciparum based on textural and morphological features

Doni Setyawan[1,4], Retantyo Wardoyo[2], Moh Edi Wibowo[2], E. Elsa Herdiana Murhandarwati[3]

[1]Doctoral Program Department of Computer Science and Electronics, Faculty of Mathematics and Natural Science,
Universitas Gadjah Mada, Yogyakarta, Indonesia
[2]Department of Computer Science and Electronics, Faculty of Mathematics and Natural Science, Universitas Gadjah Mada,
Yogyakarta, Indonesia
[3]Department of Parasitology, Faculty of Medicine, Public Health and Nursing, Universitas Gadjah Mada, Yogyakarta, Indonesia
[4]Department of Informatics, Faculty of Computer Science, Universitas Widya Dharma, Klaten, Indonesia

Article Info

ABSTRACT

Malaria is a disease caused by plasmodium parasites transmitted through the bites of female anopheles-mosquito that infect the human red blood cell (RBC). The standard malaria diagnosis is based on manual examination of a thick and thin blood smear, which heavily depends on the microscopist experience. This study proposed a system that can identify the life stages of plasmodium falciparum in human RBC. The image preprocessing process was done by illumination correction using gray world assumption, contrast enhancement using shadow correction, extraction of saturation component, and noise filtering. The segmentation process was applied using Otsu thresholding and morphological operation. The test results showed that the use of artificial neural network (ANN) using a combination of texture and morphological features gives better results when compared to the use of only texture or morphology features. The results showed that the proposed feature achieved an accuracy of 82.67%, a sensitivity of 82.18%, and a specificity of 94.17%, thus improving decision-making for malaria diagnosis.

Corresponding Author:

Retantyo Wardoyo
Department of Computer Sciences and Electronics, Universitas Gadjah Mada
55281 Building C, 4th Floor, North Sekip, Bulaksumur Yogyakarta Indonesia
Email: rw@ugm.ac.id

1. INTRODUCTION

Malaria is a disease caused by plasmodium parasites transmitted by the bites of infected female Anopheles mosquito and infect the human red blood cell (RBC). Malaria remains a significant burden on global health. In 2018, the World Health Organization (WHO) reported there were 228 million cases of malaria that occurred worldwide and an estimated 405,000 deaths from malaria [1]. Typically, the first symptoms of malaria are a high temperature of 38 °C or above, headaches, muscle pains, and diarrhea. However, these symptoms are often mild and can be challenging to identify as malaria [2]. There are five parasites of plasmodium that cause malaria in humans, i.e., plasmodium falciparum, plasmodium vivax, plasmodium malariae, plasmodium ovale, and plasmodium knowlesi. Each plasmodium in human RBC has three life stages, i.e., trophozoite, schizont, and gametocyte. Plasmodium falciparum and plasmodium vivax are the most cause of malaria cases in the world, and the most responsible for global death in the world is plasmodium falciparum [3]. Plasmodium ovale causes a not severe infection, while plasmodium malariae can cause severe fever, but it does not cause mortality [4].

The standard malaria diagnosis is typically based on a microscopic thick and thin blood smear examination. Thick blood smears assist in detecting the presence of parasites, while thin blood smears assist in identifying the species of the parasite causing the infection [5]. The diagnostic accuracy heavily depends on microscopist skill and can be strongly affected by the inter-observer variability [6]. Therefore, the experience and expertise of malaria microscopists are crucial in assuring parasite identification in human RBC [7], [8]. Some previous research has developed an automatic system to segment malaria parasites in digital microscopic blood smears. Maysanjaya *et al.* [9] proposed an approach to segment the form of parasitic cells of plasmodium vivax using the combination of the red (R) channel in the red, blue, and green (RGB) color space and saturation (S) channel in the hue, saturation, value (HSV) color space. These two-color channels are then combined to form a grayscale image. The grayscale image is then converted to a binary image using the Otsu method and morphological operation. Aggarwal *et al.* [10] have also used the Otsu method to separate the segmented images containing the infected cell from the green channel image. The experiment results in an accuracy of up to 93%.

Many researchers have also researched feature extraction and plasmodium classification. Nugroho *et al.* [11] proposed a technique to classify three stages of plasmodium falciparum, i.e., trophozoite, schizont, and gametocyte, then multilayer perceptron backpropagation algorithm is used to classify its life stages. The results show that the proposed method achieves an accuracy of 87.8%, specificity of 90.8%, and sensitivity of 81.7%. Adi *et al.* [12] also use backpropagation neural networks to classify the developmental phase of plasmodium falciparum using morphological features, i.e., area ratio and eccentricity. In subsequent research, Nugroho *et al.* [13] can improve the accuracy of the multilayer perceptron method with morphological features to classify malaria parasite from a thin blood smear digital microscopic image, and the proposed system has an accuracy of 95%, the sensitivity of 93%, and the specificity of 97%. Another approach uses a k-nearest neighbor (KNN) classifier based on shape and textural features with an accuracy of 90.17% and sensitivity of 90.23% [14], while support vector machine (SVM) using only textural features can achieve an accuracy of 97.7%, the sensitivity of 97.4%, the specificity of 97.7% [15]. Based on previous studies, this paper attempts to detect the life stages of plasmodium falciparum, i.e., ring, trophozoite, schizont, and gametocyte on a digital thin blood smear. The proposed method will extract a combination of histogram-based texture and morphological features from the image of plasmodium falciparum, then use an artificial neural network to classify the life stages of plasmodium falciparum.

2. RESEARCH METHOD

The research data is digital microscopic images of thin blood smears infected by the plasmodium falciparum parasite, which is obtained from public datasets the malaria parasite image database (MP-IDB) [16] and the public health image library (PHIL) centers for disease control and prevention (CDC) [17] as shown in Figure 1. Figure 1 shows original thin blood smear images infected with plasmodium falciparum at Figure 1(a) ring, Figure 1(b) trophozoite, Figure 1(c) schizont, and Figure 1(d) gametocyte stages. These images have been acquired using a Leica DM2000 optical laboratory microscope with 100x magnification. The image resolution is 2592×1944 px and 24-bit color depth [16]. Figure 2 shows the cropping operation from the original thin blood smear image in Figure 2(a) and the region of interest (RoI) containing an infected RBC by plasmodium falciparum with resolution 250×250 px in Figure 2(b).
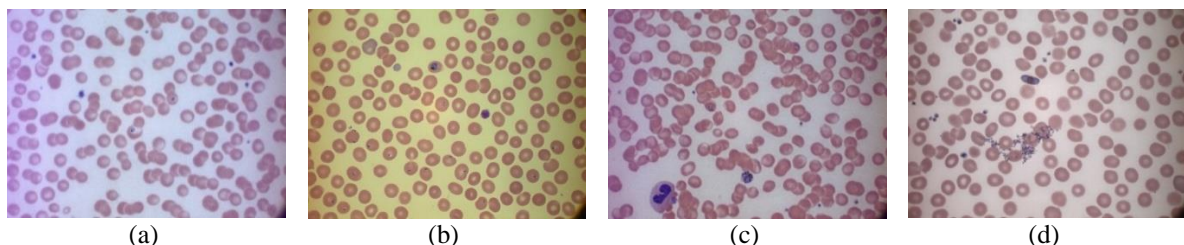

(a)   (b)   (c)   (d)

Figure 1. Digital microscopic images of thin blood smears infected by plasmodium falciparum (a) ring, (b) trophozoite, (c) schizont, and (d) gametocyte [16]

The number of datasets obtained after the cropping operation is 250 images consisting of 80 images of plasmodium falciparum at the ring stage, 65 trophozoites, 35 schizonts, and 70 gametocytes. Figure 3 shows each sample image from the Figure 3(a) ring, Figure 3(b) trophozoite, Figure 3(c) schizont, and Figure 3(d) gametocyte stages. The conducted research consists of five main steps. The first step is image

acquisition as described previously, and the examples of resulting images are shown in Figure 3. The following steps are image preprocessing, segmentation, feature extraction, and classification, as shown in Figure 4. Each of these steps is explained in the following subsections.
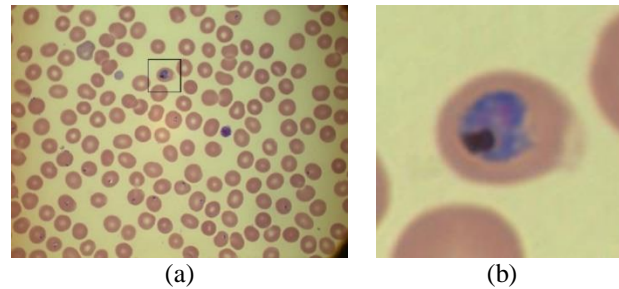

Figure 2. Cropping operation (a) original image and (b) RoI of infected RBC by plasmodium falciparum
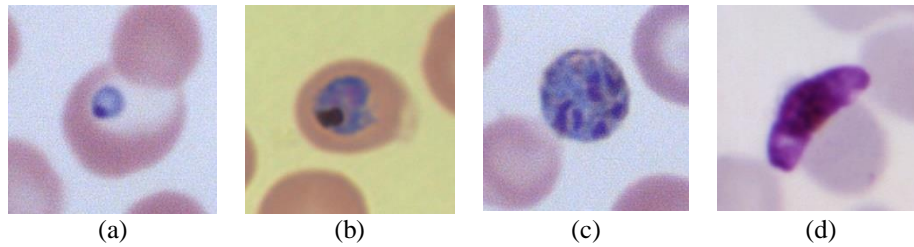

Figure 3. Life Stages of the plasmodium falciparum (a) ring, (b) trophozoite, (c) schizont, and (d) gametocyte

2.1. Preprocessing
Figures 3(a) to 3(d) shows that each image has different illumination because of the staining variability on thin blood smear and different light sources in the camera during the image acquisition process [18]. Improper handling of slides can also cause noise, resulting in the low quality of the microscopic image [19]. The main objectives of the preprocessing step are to correct illumination, improve image quality by adjusting the image contrast, and reduce the noise in the images [4]. The preprocessing stage consists of illumination correction, contrast enhancement, extraction of saturation component, and noise filtering.

2.1.1. Illumination correction
The first step in preprocessing stage is illumination correction which aims to overcome the non-uniform illumination in the image. This research uses the gray world assumption technique to correct illumination [18], [20]. The following is a mathematical representation of the gray world assumption: $f(x,y)$ is an image of infected RBC by plasmodium falciparum with size $M \times N$. $f_r(x,y)$, $f_g(x,y)$, and $f_b(x,y)$ are the red, green, and blue channels of $f(x,y)$, respectively. The average value of each channel can be computed using (1)-(3).

$$F_{ravg} = \frac{1}{MN}\sum_{x=1}^{M}\sum_{y=1}^{N} f_r(x,y) \tag{1}$$

$$F_{gavg} = \frac{1}{MN}\sum_{x=1}^{M}\sum_{y=1}^{N} f_g(x,y) \tag{2}$$

$$F_{bavg} = \frac{1}{MN}\sum_{x=1}^{M}\sum_{y=1}^{N} f_b(x,y) \tag{3}$$

In this technique, the average value of the green channel is used to compute the gain for the red and blue channels using (4) and (5).

$$g_r = \frac{F_{gavg}}{F_{ravg}} \tag{4}$$

$$g_b = \frac{F_{gavg}}{F_{bavg}} \tag{5}$$

Subsequently, g_r and g_b are used to calculate the adjusted red and blue channels using (6) and (7).

$$f_{radj}(x, y) = g_r \times f_r(x, y) \tag{6}$$

$$f_{badj}(x, y) = g_b \times f_b(x, y) \tag{7}$$

The image resulting from the gray world assumption is obtained by combining the $f_{radj}(x, y)$, $f_g(x, y)$, and $f_{badj}(x, y)$ channels.
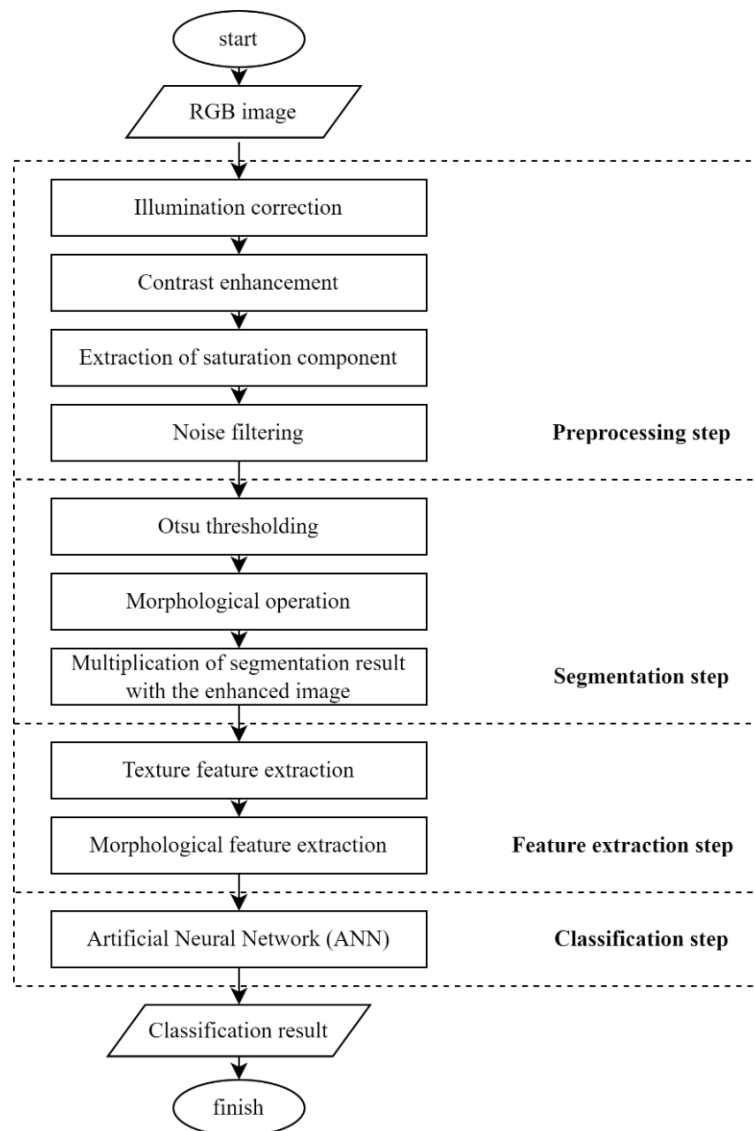

Figure 4. The proposed system for classification stadium plasmodium falciparum

2.1.2. Contrast enhancement

Contrast enhancement is conducted to increase the contrast of the image so that the plasmodium parasite object is seen more clearly. Several methods for contrast enhancement have been applied in previous studies. Here we have considered one scan shadow compensation to improve the image's contrast [21]. The approach uses a contrast stretching technique based on the image's statistical values and is applied using a logarithmic image processing model and recursive filtering. The method can improve low-light areas while

preserving colors and details and producing no visual artifacts. The algorithm consists of three steps: white balance compensation, shadow correction, and pixel amplification. The compensation for white balance is an optional step. This step adjusts the local image content based on the global intensities of the color components, with the green component serving as a reference. Suppose $I(i,j,1)$, $I(i,j,2)$, and $I(i,j,3)$ are the pixel located at (i,j) coordinates on each colors components of red, green, and blue, respectively. A recursive filter is used to calculate a running average for each color component. For each pixel at (i,j) coordinate, we calculate:

$$\bar{R}(i,j) = \beta\bar{R}(i,j-1) + (1-\beta)I(i,j,1) \tag{8}$$

$$\bar{G}(i,j) = \beta\bar{G}(i,j-1) + (1-\beta)I(i,j,2) \tag{9}$$

$$\bar{B}(i,j) = \beta\bar{B}(i,j-1) + (1-\beta)I(i,j,3) \tag{10}$$

In the (8)-(10), β is a tuning coefficient with values ranging from 0 to 1. Then, using the green color component as a reference, the correction values for each pixel in red and blue components are calculated using (11) and (12).

$$\gamma_R(i,j) = \frac{\bar{G}(i,j)}{\bar{R}(i,j)}\left(\frac{(1-\alpha)\bar{R}(i,j)+255\alpha}{(1-\alpha)\bar{G}(i,j)+255\alpha}\right) \tag{11}$$

$$\gamma_B(i,j) = \frac{\bar{G}(i,j)}{\bar{B}(i,j)}\left(\frac{(1-\alpha)\bar{B}(i,j)+255\alpha}{(1-\alpha)\bar{G}(i,j)+255\alpha}\right) \tag{12}$$

The values for γ_R and γ_B are limited to the range [0.95…1.05] and α is a tuning coefficient with values ranging from 0 to 1. The final results of adjustment pixel values $F(i,j)$ using white balance compensation are computed using (13)-(15).

$$F(i,j,1) = \gamma_R I(i,j,1) \tag{13}$$

$$F(i,j,2) = I(i,j,2) \tag{14}$$

$$F(i,j,3) = \gamma_B I(i,j,3) \tag{15}$$

The next step after white balance compensation is core processing called shadow correction. This step computes an amplification factor for each pixel that is adaptive to the average intensity of the neighboring pixel. The amplification factor is calculated using (16).

$$H(i,j) = p \cdot H(i,j-1) + (1-p)\left((1-\alpha) + \frac{255\alpha}{Y(i,j)}\right) \tag{16}$$

In (16), p represents the pole of the recursive filter, and the value is in the range [0,1]. $Y(i,j)$ is either the luminance of the pixel (i,j) in the YCbCr color space or the pixel average located at (i,j) from each color component in the RGB color space. The last step is pixel amplification using logarithmic image processing (LIP), as presented in (17). The use of the LIP model ensures that the range of the image components is preserved [22], [23].

$$F_{out}(i,j,k) = M - M\left(1 - \frac{F(i,j,k)}{M}\right)^{H(i,j)} \tag{17}$$

M is the maximum value of each component in the RGB or YCbCr color space. In the case of RGB images, the value of M is 255. k denotes the color component index, 1 for red, 2 for green, and 3 for blue.

2.1.3. Extraction of saturation component

Based on Anggraini *et al.* [24], HSV color space has perception above human visual, therefore has better performance than RGB color space. The shape of plasmodium falciparum also seems more apparent in the S channel [11]. In this study, the saturation component of the HSV color space will be extracted for further processing. HSV consists of hue, saturation, and value components. The conversion of RGB to HSV color space can use (18)-(20) [9].

$$H = \tan\left(\frac{3(G-B)}{(R-G)+(R-B)}\right) \tag{18}$$

$$S = 1 - \frac{\min(R,G,B)}{V} \tag{19}$$

$$V = \frac{R+G+B}{3} \tag{20}$$

2.1.4. Noise filtering

The noise in the image can make the image quality low, which will also impact the accuracy of segmentation of the form of plasmodium falciparum in red blood cells. Filtering techniques can be used to remove noise in the image. Based on Devi *et al.* [25], [26] this study uses median filtering to remove noise that appears in the image of plasmodium falciparum.

2.2. Segmentation

Segmentation is applied to separate the parasite plasmodium falciparum from its background. The segmentation process is done by using Otsu thresholding. Otsu method works based on the image's pixel intensity to find the optimum threshold value. Iteration will be done for all the possible values and calculate the measure's spread for the pixel levels on each side of the threshold, i.e., the pixels that fall in the background or foreground. The objective is to find the threshold value where the spread of background and foreground summation is minimum [27]. The opening morphological operation followed by the closing operation is then conducted to achieve better segmentation results [28].

2.3. Feature extraction

The objective of feature extraction is to get meaningful and useful information from the raw pixel values of an image. In this research, two types of features are combined, first is the histogram-based texture consists of mean, standard deviation, skewness, energy, entropy, and smoothness [11]. The second is morphological features, i.e., area ratio and eccentricity [12]. Mean is the average measurement of all pixel intensities in the image, which can be computed using (21):

$$mean = \sum_{i=0}^{L-i} i.p(i) \tag{21}$$

where i is the grayscale value, $p(i)$ is the probability of i in the image, and L is the maximum grayscale value. Standard deviation is the variation measurement of the image's pixel intensities, which is calculated by (22), where μ is the mean value. This feature gives the measure of the contrast.

$$standar\ deviation = \sqrt{\sum_{i=0}^{L-1}(i-\mu)^2\,p(i)} \tag{22}$$

Energy is the measurement of pixel intensities distribution with grayscale range value, energy is the uniformity in an image and can be calculated by (23).

$$energy = \sum_{i=0}^{L-1}[p(i)]^2 \tag{23}$$

Skewness is the asymmetry measurement of the pixel values toward the mean. The negative value indicates that the intensity distribution is leaning to the left, whereas the positive value indicates that the intensity distribution is leaning to the right. Skewness can be calculated by (24).

$$skewness = \sum_{i=0}^{L-1}(i-\mu)^3 p(i) \tag{24}$$

Entropy indicates the level of image complexity. High complexity images will have high entropy values too, and entropy also shows the amount of information contained in the data distribution. Entropy can be calculated by (25).

$$entropy = -\sum_{L-0}^{L-1} p(i)log_2(p(i)) \tag{25}$$

Smoothness measures the level of smoothness or roughness of image intensity, calculated by (7), where σ is the standard deviation. The low value of smoothness indicates the image has a roughness of intensity. Smoothness can be calculated by (26).

$$smoothness = 1 - \frac{1}{1+\sigma^2} \tag{26}$$

Area ratio is the ratio between the number of pixels that form an object and the number of overall pixels of an image. Eccentricity is the comparison between the length of minor and major axes, eccentricity can be calculated by (27) and illustrated in Figure 5.

$$eccentricity = \sqrt{1 - \left(\frac{b}{a}\right)^2} \tag{27}$$
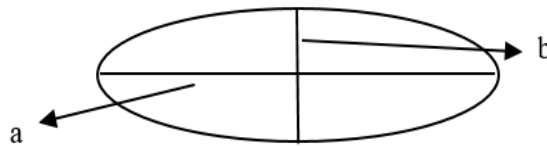
Figure 5. Illustration of eccentricity

2.4. Classification

In this study, artificial neural network (ANN) is used to classify the input image into four classes, i.e. ring, trophozoite, schizont, and gametocyte classes. The selection of ANN is based on previous research, that ANN provides the best accuracy compared to other methods such as naive Bayes, logistic regression, classification and regression tree, SVM, and KNN [19], [25], [29]. The built ANN architecture consists of three parts, namely input, hidden, and output layers, as shown in Figure 6.
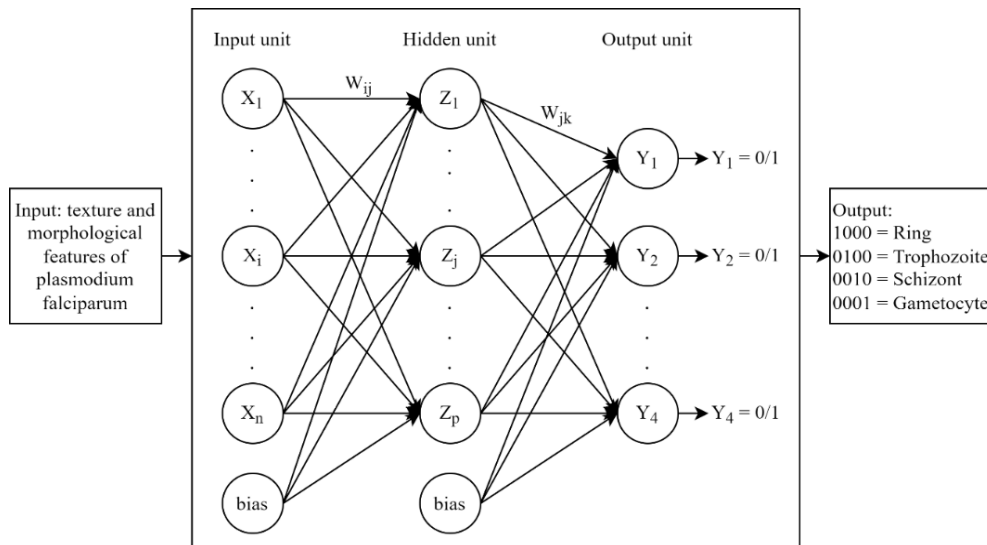
Figure 6. ANN architecture

In this study, only one hidden layer is used. The use of one hidden layer is sufficient to estimate the continuous mapping from the input pattern to the output pattern until the classification results are obtained [30]. The input for ANN is the value of each feature from the feature extraction process. The number of features used will determine the number of neurons in the input layer, while the number of neurons in the hidden layer is calculated based on (28) [31].

$$H = \sqrt{(m+2)N} + 2\sqrt{N/(m+2)} \tag{28}$$

In (28), H states the number of hidden nodes in the hidden layer, N is the number of nodes in the input layer, and m is the number of nodes in the output layer. In the output layer, the number of neurons used is equal to

the number of classes that are the output of the classification process. The performance of the classification tasks will be measured with its accuracy, sensitivity, and specificity.

3.   RESULTS AND DISCUSSION

In the preprocessing step, the input is the RGB image, as shown in Figure 3. The preprocessing process begins with illumination correction, contrast enhancement, extraction of saturation component, and the last is noise reduction using median filtering. Figure 7 shows the resulting image of the illumination correction using the gray world assumption for the 7(a) ring, 7(b) trophozoite, 7(c) schizont, and 7(d) gametocyte stages of plasmodium falciparum.

| (a) | (b) | (c) | (d) |
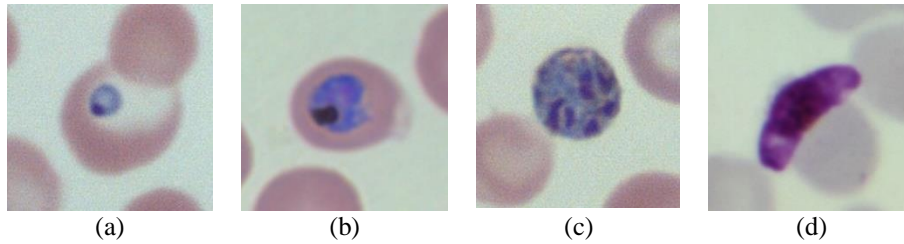
Figure 7. The resulting image of illumination correction (a) ring, (b) trophozoite, (c) schizont, and (d) gametocyte

It can be seen that the illumination corrected image has a more uniform illumination between one image and another, as shown in Figures 7(a)-(d). Images with uniform illumination can make determining the threshold in the segmentation process more straightforward, and the texture feature extraction process becomes more objective than the non-uniform illumination image. Next, the contrast enhancement is performed using the one scan shadow compensation method. This study used the value of $p = 0.125$ and $\alpha = 0.125$ to calculate the amplification factor. If $p > 0.5$, visible artifacts can appear in high contrast areas, and if $\alpha > 0.25$, noise becomes visible in low-quality images [21]. Figure 8 shows the amplification factor map generated from Figures 7(a)-(d). Amplification factor maps for the ring, trophozoite, schizont, and gametocyte are shown in Figures 8(a)-(d), respectively. Figure 9 shows the contrast enhancement results for the ring, trophozoite, schizont, and gametocyte in Figures 9(a)-(d), respectively.
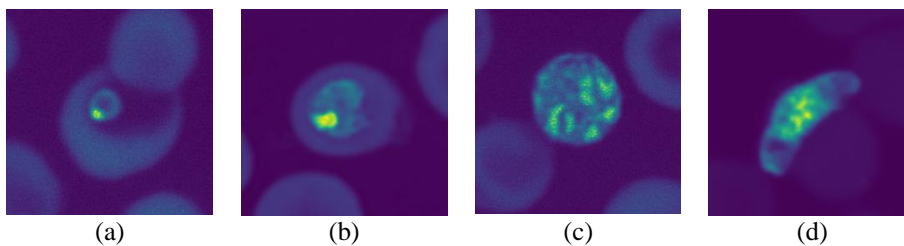

| (a) | (b) | (c) | (d) |

Figure 8. The amplification factor map (a) ring, (b) trophozoite, (c) schizont, and (d) gametocyte
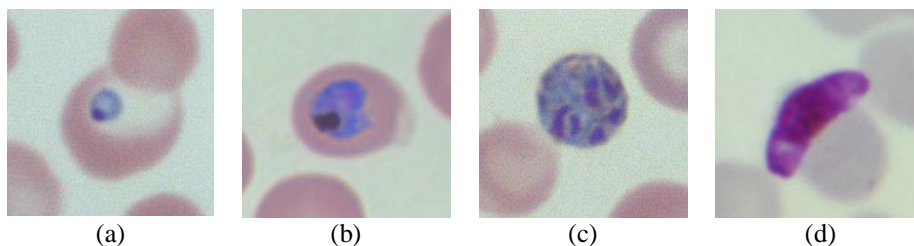

| (a) | (b) | (c) | (d) |

Figure 9. The resulting image of contrast enhancement (a) ring, (b) trophozoite, (c) schizont, and (d) gametocyte

In Figure 8, it can be seen that the amplification factors are adapted to each pixel based on the content local of the image. Using a recursive filter in amplification factor calculation makes the transition from one pixel to the next smoother and can reduce the artifacts [21]. Figure 10 displays histograms of the image before and after contrast enhancement. Figure 10(a) represents the histogram from the image in Figure 7(d), and Figure 10(b) represents the histogram from the image in Figure 9(d).

In Figures 9 and 10, it can be seen that the darker areas are enhanced, so the details become more visible in the dark areas and maintain a near-constant intensity in lighter areas. After increasing the contrast, the HSV color space conversion is performed to obtain the saturation component. Figure 11 shows the result of HSV conversion from the RGB image. The HSV image of gametocyte plasmodium falciparum is shown in Figure 11(a), while the hue, saturation, and value components are shown in Figures 11(b)-(d), respectively. Figure 12 shows the 3D scatter plot for the HSV image of plasmodium falciparum gametocyte.
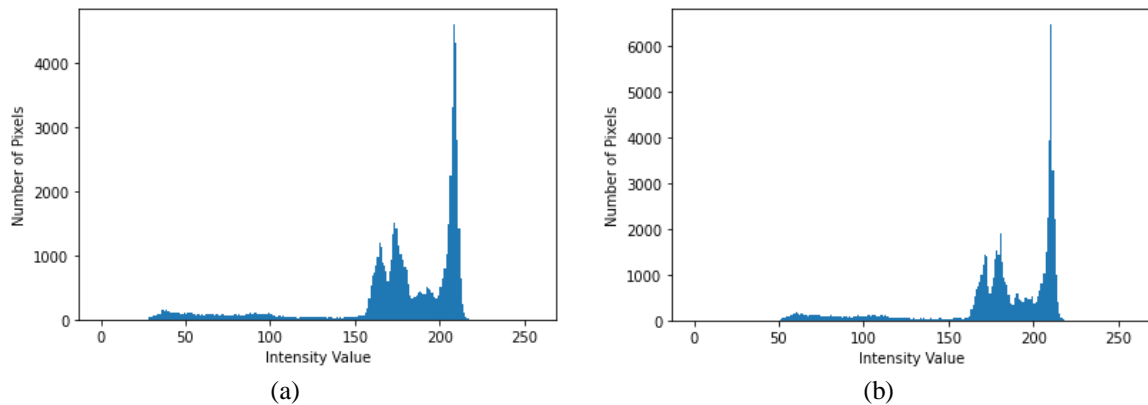

(a)   (b)

Figure 10. Image histogram comparison between (a) before contrast enhanced and (b) after contrast enhanced using shadow compensation method

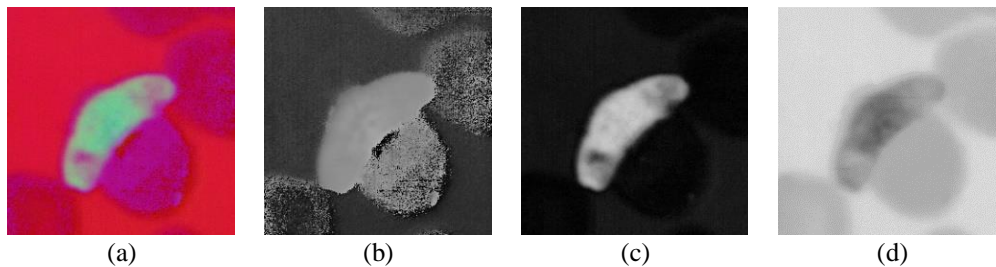(a)   (b)   (c)   (d)

Figure 11. The HSV image of gametocyte plasmodium falciparum (a) HSV image, (b) hue component, (c) saturation component, and (d) value component
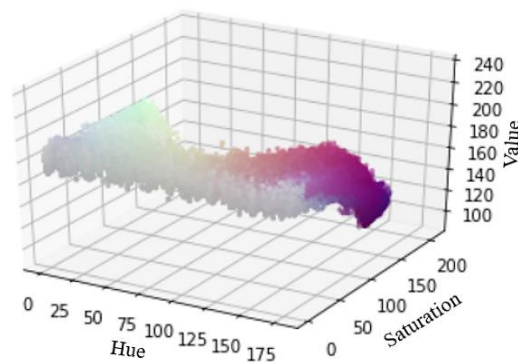

Figure 12. 3D scatter plot for the HSV image of plasmodium falciparum gametocyte

By looking at Figure 11, plasmodium falciparum cells are more visible in the saturation component. In Figure 12, it is seen that the plots on the graph lie in a small range along the saturation axis. Based on the results of this experiment, the saturation component is selected for the following process. The last step of the preprocessing stage is the use of median filtering to remove noise. In this study, the filter size used is 3×3. The use of a larger filter size can make the image blur. The filtered image will be input for the segmentation stage, which consists of steps, conversion to a binary image, morphological operations, and multiplication with the contrast-enhanced image, as shown in Figure 13.

Figure 13(a) is the input for the segmentation process. The result of binary conversion using Otsu thresholding still leaves a hole in the plasmodium object, as shown in Figure 13(b). Therefore, a morphological closing operation is performed to close the hole in the object. A morphological opening operation is also carried out if the image contains small objects other than plasmodium. The result of the morphological operation is presented in Figure 13(c). The result segmentation process was obtained by multiplying the binary image in Figure 13(c) with the enhanced image in Figure 9(d). Figure 13(d) shows the final output of the segmentation process.

The image resulting from the segmentation process will be the input for the feature extraction stage. The extracted texture features are mean, standard deviation, skewness, energy, entropy, and smoothness [11], while the extracted morphological features are area ratio and eccentricity [12]. Figure 14 shows the values for each feature extracted from the image of plasmodium falciparum in gametocyte stadium.
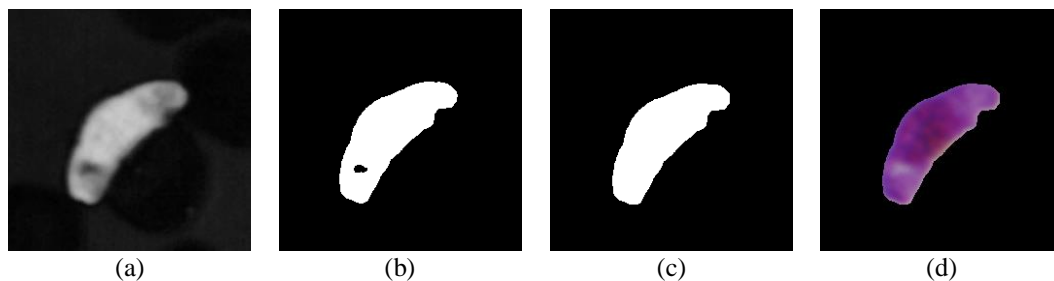
(a)	(b)	(c)	(d)

Figure 13. Segmentation process (a) filtered image, (b) binary conversion, (c) morphological operation, and (d) the final segmentation result

- Mean 88.390518
- Standard deviation 24.649282
- Skewness 0.511578
- Energy 0.013027
- Entropy 4.481055
- Smoothness 0.998357
- Area ratio 0.113168
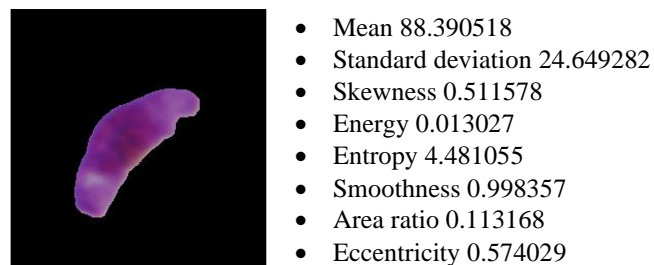- Eccentricity 0.574029

Figure 14. The values for each extracted feature from the plasmodium falciparum gametocyte image

The next step is the classification of plasmodium falciparum into the ring, trophozoite, schizont, and gametocyte classes. Two processes are carried out at the classification stage, namely training and testing the built model. From a total of 250 image datasets, it is divided into training data of 175 images and testing data of 75. The first model uses texture features from research [11], the second model uses morphological features from research [12], and the third is the proposed model by combining texture and morphological features. The number of hidden nodes in the hidden layer is obtained based on (28). Table 1 shows the three architectures of the built ANN model. The parameters used in the training process are the learning rate 0.10, the momentum 0.2, and the number of epochs 500. Tables 2 and 3 show the model classification performance with the proposed feature set and the existing feature set in [11] and [12].

Based on the experimental results presented in Tables 2 and 3, the use of a combination of texture and morphological features is proven to provide better performance when compared to using only texture or morphological features. The average sensitivity and specificity using a combination of texture and shape features give better results when compared to using only texture or morphological features. The average

sensitivity when using a combination of texture and morphological features is 82.18% while using only texture or morphological features is 71.03% and 75.87%, respectively. The average specificity when using a combination of texture and morphological features is 94.17% while using only texture or morphological features is 90.59% and 91.83%, respectively. The accuracy when using a combination of texture and morphological features also gives a better result, which is 82.67%, while using only texture and morphological features is 72.00% and 76.00%, respectively. Using a combination of texture and morphological features can increase accuracy by 10.67% compared to using only texture features and can increase accuracy by 6.67% compared to using only morphological features.

Table 1. Comparison of the built ANN architecture

Model	Feature	Number of features	Number of nodes		
			Input layer	Hidden layer	Output layer
1.	Mean, standard deviation, skewness, energy, entropy, and smoothness [11]	6	6	8	4
2.	Area ratio and eccentricity [12]	2	2	5	4
3.	Mean, standard deviation, skewness, energy, entropy, smoothness, area ratio, and eccentricity (proposed features)	8	8	9	4

Table 2. Classification performance of the proposed and existing feature set in the previous literature

Class	Sensitivity (%)			Specificity (%)		
	Texture [11]	Morphological [12]	Proposed feature	Texture [11]	Morphological [12]	Proposed feature
Ring	80.95	95.24	76.19	87.04	75.93	94.44
Trophozoite	63.16	31.58	84.21	91.07	98.21	85.71
Schizont	60.00	86.67	73.33	93.33	95.00	98.33
Gametocyte	80.00	90.00	95.00	90.91	98.18	98.18
Average of all classes	71.03	75.87	82.18	90.59	91.83	94.17

Table 3. Comparison of model accuracy with proposed and existing feature set

Accuracy (%)		
Texture [11]	Morphological [12]	Proposed feature
72.00	76.00	82.67

4. CONCLUSION

The study presented in this research focuses on identifying life stage Plasmodium falciparum species. The approach consists of image preprocessing using gray world assumption for illumination correction, shadow correction for contrast enhancement, extraction of saturation component from HSV color space, and median filtering. The segmentation process is applied using Otsu thresholding and morphological operation on the saturation component. The use of a combination of texture and morphological features provides better performance on the classification results when compared to using only texture or morphological features. The classification performance using combination texture and morphological features results in an accuracy of 82.67%, a sensitivity of 82.18%, and a specificity of 94.17%. The development of the research is necessary to increase classification performance. The improvement can be made by adding other features and selecting features to filter just the relevant feature.

REFERENCES

[1] WHO, "World malaria report 2019," *World Health Organization*, 2019. https://www.who.int/news-room/feature-stories/detail/world-malaria-report-2019 (accessed Dec. 18, 2019).

[2] NHS, "Symptoms malaria," *National Health Service*. https://www.nhs.uk/conditions/malaria/symptoms (accessed Dec. 18, 2019).

[3] M. Poostchi, K. Silamut, R. J. Maude, S. Jaeger, and G. Thoma, "Image analysis and machine learning for detecting malaria," *Translational Research*, vol. 194, pp. 36–55, Apr. 2018, doi: 10.1016/j.trsl.2017.12.004.

[4] Z. Jan, A. Khan, M. Sajjad, K. Muhammad, S. Rho, and I. Mehmood, "A review on automated diagnosis of malaria parasite in microscopic blood smears images," *Multimedia Tools and Applications*, vol. 77, no. 8, pp. 9801–9826, Mar. 2018, doi:

10.1007/s11042-017-4495-2.

[5]   DPDx, "Blood specimens-microscopic examination," *Center for Disease Control and Prevention*. https://www.cdc.gov/dpdx/diagnosticprocedures/blood/microexam.html (accessed Dec. 18, 2016).

[6]   K. Mitiku, G. Mengistu, and B. Gelaw, "The reliability of blood film examination for malaria at the peripheral health unit," *Ethiopian Journal of Health Development*, vol. 17, no. 3, pp. 197–204, 2003

[7]   A. Mehrjou, T. Abbasian, and M. Izadi, "Automatic malaria diagnosis system," in *2013 First RSI/ISM International Conference on Robotics and Mechatronics (ICRoM)*, Feb. 2013, pp. 205–211., doi: 10.1109/ICRoM.2013.6510106.

[8]   F. E. Mckenzie, J. Sirichaisinthop, R. S. Miller, J. Robert A. Gasser, and C. Wongsrichanalai, "Dependence of malaria detection and species diagnosis by microscopy on parasite density," *The American Journal of Tropical Medicine and Hygiene*, vol. 69, no. 4, pp. 372–376, Oct. 2003, doi: 10.4269/ajtmh.2003.69.372.

[9]   I. M. D. Maysanjaya, H. A. Nugroho, N. A. Setiawan, and E. E. H. Murhandarwati, "Segmentation of Plasmodium vivax phase on digital microscopic images of thin blood films using colour channel combination and Otsu method," in *AIP Conference Proceedings*, 2016, vol. 1755., doi: 10.1063/1.4958595.

[10]   P. Aggarwal, A. Khatter, and G. Vyas, "An intensity threshold based image segmentation of malaria infected cells," in *2018 Second International Conference on Computing Methodologies and Communication (ICCMC)*, Feb. 2018, pp. 549–553., doi: 10.1109/ICCMC.2018.8487494.

[11]   H. A. Nugroho, S. A. Akbar, and E. E. H. Murhandarwati, "Feature extraction and classification for detection malaria parasites in thin blood smear," in *2015 2nd International Conference on Information Technology, Computer, and Electrical Engineering (ICITACEE)*, Oct. 2015, pp. 197–201., doi: 10.1109/ICITACEE.2015.7437798.

[12]   K. Adi, S. Pujiyanto, R. Gernowo, A. Pamungkas, and A. B. Putranto, "Identifying the developmental phase of plasmodium falciparum in malaria-infected red blood cells using adaptive color segmentation and back propagation neural network," *International Journal of Applied Engineering Research*, vol. 11, no. 15, pp. 8754–8759, 2016

[13]   H. A. Nugroho, A. Darojatun, I. Ardiyanto, and R. L. B. Buana, "Classification of plasmodium malariae dan plasmodium ovale in microscopic thin blood smear digital images," *International Journal on Advanced Science, Engineering and Information Technology*, vol. 8, no. 6, Dec. 2018, doi: 10.18517/ijaseit.8.6.6514.

[14]   A. Nanoti, S. Jain, C. Gupta, and G. Vyas, "Detection of malaria parasite species and life cycle stages using microscopic images of thin blood smear," in *2016 International Conference on Inventive Computation Technologies (ICICT)*, Aug. 2016, vol. 1, pp. 1–6., doi: 10.1109/INVENTIVE.2016.7823258.

[15]   V. K. Bairagi and K. C. Charpe, "Comparison of texture features used for classification of life stages of malaria parasite," *International Journal of Biomedical Imaging*, vol. 2016, pp. 1–9, 2016, doi: 10.1155/2016/7214156.

[16]   A. Loddo, C. Di Ruberto, M. Kocher, and G. Prod'Hom, "MP-IDB: the malaria parasite image database for image processing and analysis," in *Lecture Notes in Computer Science (including subseries Lecture Notes in Artificial Intelligence and Lecture Notes in Bioinformatics)*, vol. 11379, Springer International Publishing, 2019, pp. 57–65., doi: 10.1007/978-3-030-13835-6_7.

[17]   PHIL, "Public health image library," *Center for Disease Control and Prevention*. 2017. https://phil.cdc.gov/default.aspx (accessed Nov. 2, 2019).

[18]   D. K. Das, M. Ghosh, M. Pal, A. K. Maiti, and C. Chakraborty, "Machine learning approach for automated screening of malaria parasite using light microscopic images," *Micron*, vol. 45, pp. 97–106, Feb. 2013, doi: 10.1016/j.micron.2012.11.002.

[19]   D. K. Das, A. K. Maiti, and C. Chakraborty, "Automated system for characterization and classification of malaria-infected stages using light microscopic images of thin blood smears," *Journal of Microscopy*, vol. 257, no. 3, pp. 238–252, Mar. 2015, doi: 10.1111/jmi.12206.

[20]   E. Y. Lam, "Combining gray world and retinex theory for automatic white balance in digital photography," in *Proceedings of the Ninth International Symposium on Consumer Electronics (ISCE 2005)*, 2005, pp. 134–139., doi: 10.1109/ISCE.2005.1502356.

[21]   F. Albu, C. Vertan, C. Florea, and A. Drimbarean, "One scan shadow compensation and visual enhancement of color images," in *2009 16th IEEE International Conference on Image Processing (ICIP)*, Nov. 2009, pp. 3133–3136, doi: 10.1109/ICIP.2009.5414437.

[22]   M. Jourlin and J. C. Pinoli, "Logarithmic image processing: the mathematical and physical framework for the representation and processing of transmitted images," in *Advances in Imaging and Electron Physics*, vol. 115, no. C, Elsevier, 2001, pp. 129–196, doi: 10.1016/S1076-5670(01)80095-1.

[23]   W. Wang and B. Zhang, "An improved visual enhancement method for color images," in *Fifth International Conference on Digital Image Processing (ICDIP 2013)*, Jul. 2013, vol. 8878, doi: 10.1117/12.2031774.

[24]   D. Anggraini, A. S. Nugroho, C. Pratama, I. E. Rozi, A. A. Iskandar, and R. N. Hartono, "Automated status identification of microscopic images obtained from malaria thin blood smears," in *Proceedings of the 2011 International Conference on Electrical Engineering and Informatics*, Jul. 2011, pp. 1–6, doi: 10.1109/ICEEI.2011.6021762.

[25]   S. S. Devi, S. A. Sheikh, A. Talukdar, and R. H. Laskar, "Malaria infected erythrocyte classification based on the histogram features using microscopic images of thin blood smear," *Indian Journal of Science and Technology*, vol. 9, no. 45, Dec. 2016, doi: 10.17485/ijst/2016/v9i45/94119.

[26]   S. S. Devi, J. Singha, M. Sharma, and R. H. Laskar, "Erythrocyte segmentation for quantification in microscopic images of thin blood smears," *Journal of Intelligent and Fuzzy Systems*, vol. 32, no. 4, pp. 2847–2856, Mar. 2017, doi: 10.3233/JIFS-169227.

[27]   N. Otsu, "A threshold selection method from gray-level histograms," *IEEE Transactions on Systems, Man, and Cybernetics*, vol. 9, no. 1, pp. 62–66, Jan. 1979, doi: 10.1109/TSMC.1979.4310076.

[28]   H. A. Nugroho, M. S. Wibawa, N. A. Setiawan, E. E. H. Murhandarwati, and R. L. B. Buana, "Identification of plasmodium falciparum and plasmodium vivax on digital image of thin blood films gf," *Indonesian Journal of Electrical Engineering and Computer Science (IJEECS)*, vol. 13, no. 3, pp. 933–944, Mar. 2019, doi: 10.11591/ijeecs.v13.i3.pp933-944.

[29]   S. S. Devi, R. H. Laskar, and S. A. Sheikh, "Hybrid classifier based life cycle stages analysis for malaria-infected erythrocyte using thin blood smear images," *Neural Computing and Applications*, vol. 29, no. 8, pp. 217–235, Apr. 2018, doi: 10.1007/s00521-017-2937-4.

[30]   L. Fausett, *Fundamentals of neural network: architectures, algorithms, and applications*. 1st edition, Pearson, 1994.

[31]   G.-B. Huang, "Learning capability and storage capacity of two-hidden-layer feedforward networks," *IEEE Transactions on Neural Networks*, vol. 14, no. 2, pp. 274–281, Mar. 2003, doi: 10.1109/TNN.2003.809401.

BIOGRAPHIES OF AUTHORS

Doni Setyawan completed his Bachelor's degree in Informatics Engineering, Universitas Ahmad Dahlan (2008), and his Master's degree in the Department of Computer Science and Electronics, Faculty of Mathematics and Natural Science, Universitas Gadjah Mada (2016). He works as a Lecturer in the Department of Informatics, Faculty of Computer Science, Unwidha, Klaten, Indonesia. Currently, he is pursuing his doctoral program in the Department of Computer Science and Electronics, Faculty of Mathematics and Natural Science, UGM, Yogyakarta, Indonesia. He can be contacted at email: doniset@mail.ugm.ac.id.

Retantyo Wardoyo completed his Bachelor's degree in Mathematics from Universitas Gadjah Mada (1982). In 1990, he obtained his Master's degree in Computer Science at the University of Manchester, UK, and in 1996 he received his doctoral degree from Computation at the University of Manchester Institute of Sciences and Technology, UK. Currently, he is a lecturer and a researcher at the Department of Computer Science and Electronics, Universitas Gadjah Mada. His research interests include intelligent systems, reasoning systems, expert systems, fuzzy systems, vision systems, Group DSS & Clinical DSS, medical computing and computational intelligence. He can be contacted at email: rw@ugm.ac.id.

Moh Edi Wibowo has completed his bachelor's degree in the Department of Computer Science and Electronics, Universitas Gadjah Mada, Indonesia. He received his master's degree from the Department of Computer Science and Electronics, Faculty of Mathematics & Natural Science, Universitas Gadjah Mada (2006). His doctoral degree is from Computer Vision and Pattern Recognition, Queensland University of Technology, Australia. Currently, he is a lecturer and a researcher at the Department of Computer Science and Electronics, Universitas Gadjah Mada. His research interests include intelligent systems, algorithms and computation, image processing, and computer vision. He can be contacted at email: mediw@ugm.ac.id.

E. Elsa Herdiana Murhandarwati completed her Bachelor's degree (1993) and Master's degree (1996) in Universitas Gadjah Mada. In 2011, she received her Ph.D. in Medical Science at Monash University. Currently, she is a Lecturer in the Department of Parasitology Faculty of Medicine, Public Health and Nursing Universitas Gadjah Mada. Her research interest includes tropical medicine and computer-aided diagnostic for malaria disease. She can be contacted at email: elsa.herdiana@ugm.ac.id.